Available online at www.sciencedirect.com
ScienceDirect
Thermochimica Acta 465 (2007) 59–66
thermochimica acta
www.elsevier.com/locate/tca

# Cold crystallization of poly(ethylene glycol)–water systems

Tatsuko Hatakeyma [a,*], Hazuki Kasuga [b], Masaru Tanaka [c], Hyoe Hatakeyama [d]

[a] *Lignocel Research, 2-6-16 Mejirodai, Bunkyo-ku, Tokyo 112-0015, Japan*
[b] *Otsuma Women's University, 12 Sanban-cho, Chiyoda-ku, Tokyo 102-8357, Japan*
[c] *Molecular Deviced Laboratory, Research Institute for Electronic Science, Hokkaido University and Japan Science and Technolgy Corporation, N12W16 Kita-ku, Sapporo 060-0812, Japan*
[d] *Fukui University of Technology, 3-6-1 Gakuen, Fukui 910-8505, Japan*

Received 6 February 2007; received in revised form 16 August 2007; accepted 20 September 2007
Available online 1 October 2007

**Abstract**

Phase transition behaviour of poly(ethylene glycol) (PEG)–water systems was investigated by differential scanning calorimetry (DSC) in a temperature range from 150 to 350 K and water content (mass of water/mass of PEG) range from 0 to 10 g g$^{-1}$. In DSC heating curves, glass transition, cold crystallization, melting of eutectic crystal, water and PEG crystal were observed depending on water content. The cold crystallization of the system, which is thought to be used as an index of biocompatibility of polymer–water interaction, received particular attention. It was found that cold crystallization and glass transition were observed in a wide water content range from 0.05 to 10 g g$^{-1}$. From the enthalpy balance of transitions in both heating and cooling DSC curves, it was confirmed that cold crystallization is attributable to the molecular rearrangement of PEG molecules associated with amorphous ice. When four water molecules are attached to one repeating unit of PEG, the heat capacity difference at glass transition temperature attains the largest value and the enthalpy of cold crystallization shows the maximum value.


*Keywords:* Poly(ethylene glycol); Water; Phase transition; Cold crystallization

## 1. Introduction

A large number of synthetic polymers having a biomembrane-like surface have been investigated in order to develop new biomedical materials [1–6]. In our previous studies, it was found that poly(2-methoxyethyl acrylate) (PMEA) shows excellent blood compatibility. It was clearly observed that the amount of adsorbed proteins onto the surface of PMEA is much lower than that of other conventional polymers. It is noteworthy that the degree of denaturation of proteins is maintained at a low level on the surface of PMEA [7–13]. PMEA has already been applied as a coating material for an oxygenators [14–16] and a cardiopulmonary bypass [17–19].

The structural change of water restrained by biomaterials which elucidates the biocompatible nature of living organs has been discussed over many years [20–22]. It is known that phase transition temperatures and enthalpies of water bound by biomaterials differ from bulk water and the difference depends on degree of association with bio-matrix [23–25]. It was found that the phase transition of water restrained by PMEA showed unique behaviour, when restrained water was measured by differential scanning calorimetry (DSC) [9,12,13]. As reported previously, unusually large cold crystallization was observed at around 220 K, which is attributable to restrained water in the above polymers. At the same time, it was found that enthalpy of cold crystallization correlates with biofunctionality, especially blood compatibility [12,13]. On this account, it is suggested that the cold crystallization peak observed by DSC has a potential to be used as an index of biological functionality.

Among a large number of polymer–water systems investigated by differential scanning calorimetry, cold crystallization is mainly observed in polysaccharide–water systems [25], such as water–galactomannan systems [26], water–xanthan gum [27], cellulose sulfate–water systems [28], water–carboxymethylcellulose [29], etc. The observed cold

* Corresponding author. Tel.: +81 776 89 2885; fax: +81 776 89 2884.
*E-mail address:* lingocel@mx3.fctv.ne.jp (T. Hatakeyma).

0040-6031/$ – see front matter © 2007 Published by Elsevier B.V.
doi:10.1016/j.tca.2007.09.005

crystallization for the polysaccharide–water systems is not sharp and the water content range is also limited compared with that found in PMEA–water systems. As well as PMEA–water systems, it is known that poly(ethylene glycol) (PEG)–water systems show a large and clear exothermic peak due to cold crystallization [30,31]. PEG is an indispensable component in order to design specific polymers containing a flexible component. Various kinds of three-dimensional polymers and biopolymers have been prepared using PEG targeting specific functionality. This is due to the fact that PEG has a simple chemical structure (H–[O–$CH_2$–$CH_2$–]$_n$–OH) and a wide range of molecular weight samples can easily be obtained. Biocompatibility, reactivity and non-toxic nature are also important factors in its wide application [32]. PEG is also blended with hydrophilic polymer in order to control the functionality [32–36]. The state of water sorbed to PEG was studied by Fourier transform infrared spectroscopy, and different kinds of sorbed water molecules, such as binding water, types of dimeric water, bridging water, etc. are identified [37]. The above water molecules are directly bound with the oxygen atoms or bridging two PEG chains.

In this study, we pay particular attention to cold crystallization observed in a special type of polymer–water system in order to elucidate water biopolymer interaction. Differential scanning calorimetry is extensively used in order to clarify the thermal histories by which cold crystallization is characteristically observed.

## 2. Experimental

### 2.1. Materials

Poly(ethylene glycol) was obtained from Polysciences Inc., (USA). PEG samples with molecular mass 1540 were used without further purification.

### 2.2. Differential scanning calorimetry

A Seiko Instruments Ltd. differential scanning calorimeter DSC200C equipped with a cooling apparatus was used. Nitrogen gas flow rate was 20 ml min$^{-1}$. Aluminium sealed type pans were weighed by a Sartorius microbalance with precision $\pm 0.1 \times 10^{-7}$ g. Samples about 3–5 mg were placed in the pans and a small amount of water was added using a micro-syringe. The water was evaporated until an appropriate amount of water was attained. Then, the sample pans were sealed hermetically using an auto sealer. Samples with added water were weighed. Samples were kept at room temperature overnight in order to confirm that no mass loss occurred and DSC measurements were carried out. The sample was heated to 350 K then, cooled to 120 K, held at 120 K for 10 min, and heated to 350 K. Cooling rates were 20–40 K min$^{-1}$, and heating rate was 10 K min$^{-1}$. Each sample was measured four times. The second cooling and heating curves were used for analysis.

The pans were pierced after DSC measurement, and then annealed at 120 °C for over 1 h in an electric oven. Water content ($W_c$) was defined as the following equation:

$$\text{water content}\,(W_c) = \frac{\text{g of water}}{\text{g of dry sample}}\,(\text{g g}^{-1}) \quad (1)$$

Glass transition temperature ($T_g$) was defined as the temperature at which the extrapolated baseline before the transition intersects the tangent drawn at the point of greatest slope on the step of the glass transition [38]. Temperature and enthalpy of crystallization and melting of the sample were calibrated using indium and pure water as a standard material. The heat capacity difference ($\Delta C_p$) at $T_g$ was calculated using the total weight of sample [39]. Peak temperature and starting temperature of each transition were assigned as crystallization temperature ($T_c$), starting temperature of crystallization ($T_{ci}$), melting temperature ($T_m$), starting temperature of melting ($T_{mi}$) and cold crystallization temperature ($T_{cc}$), respectively. When multiple transitions were observed, each transition was a number from the low- to high-temperature side. Temperature was calibrated using pure water. The starting temperatures of cooling and melting of pure water were determined as 273 K at heating rate of 10 K min$^{-1}$. Crystallization enthalpy ($\Delta H_c$), cold crystallization enthalpy ($\Delta H_{cc}$) and melting peak enthalpy ($\Delta H_m$) were also calculated using pure water as a reference material. Enthalpy was calculated using the total weight of sample, water or PEG depending on the characteristics of each transition.

## 3. Results

Fig. 1 shows the stacked DSC cooling curves of PEG (molecular mass = 1540) with various water contents in a temperature range from 353 to 150 K cooled at 10 K min$^{-1}$. As stated in the experimental section, DSC measurement was carried out four times for each sample and data obtained by the second cooling

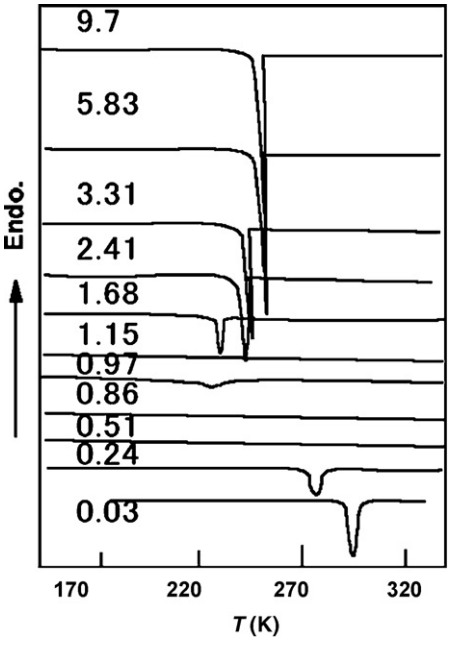


Fig. 1. DSC cooling curves of PEG–water systems. Numerals in the figure show water content ($W_c$) in g g$^{-1}$ and cooling rate = 10 K min$^{-1}$.

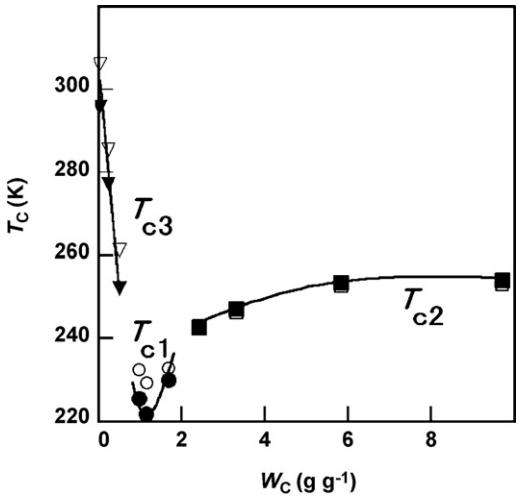


Fig. 2. Relationships between crystallization temperatures and water content. (●) Crystallization categorized into group 1; (■) group 2; (▼) group 3.

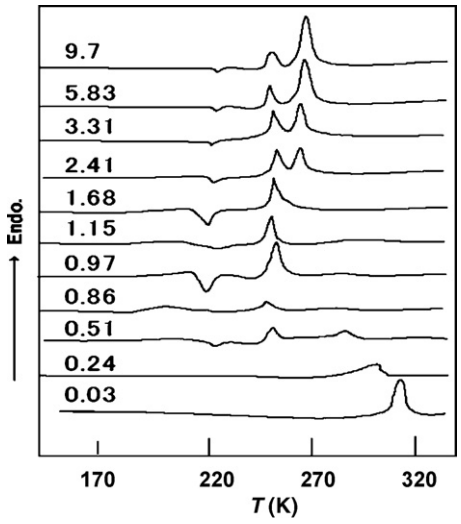


Fig. 4. DSC heating curves of PEG–water systems. Numerals in the figure show water content ($W_c$) in g g$^{-1}$ and heating rate = 10 K min$^{-1}$.

and heating run was used for analysis. In Fig. 1, an exothermic peak observed for the sample with $W_c = 0.03$ g g$^{-1}$ shifts to the low-temperature side with increasing $W_c$. No peak was observed in cooling curves when in a water content ranging from 0.51 to 0.86 g g$^{-1}$. However, when DSC curves were magnified, a small exotherm could be observed at around 220–230 K. The crystallization peak observed at around −240 K is sharp and shifts to the high-temperature side with increasing water content. From Fig. 1, three different types of crystallization are thought to occur in PEG–water systems. In this study, crystallization peaks are categorized into three groups, $T_{c1}$, $T_{c2}$ and $T_{c3}$ from the low- to high-temperature side. When the cooling curves were magnified, heat capacity difference due to glass transition was observed for the samples with water content 0.24–1.68 g g$^{-1}$. Heat capacity difference at $T_g(\Delta C_p)$ was 0.2–1.2 J g$^{-1}$ K$^{-1}$. For the calculation of heat capacity, summation of mass of PEG and water was used.

Fig. 2 shows the peak temperature and starting temperature of crystallization of three different groups as a function of water content $(W_c)_{c1}$ is observed in a narrow water content range at around 220–230 K and $T_{c2}$ increases slightly with increasing water content. $T_{c3}$ decreases markedly compared with those of the other two groups. Enthalpies of crystallization calculated from the peak area are shown in Fig. 3 as a function of water content. In order to calculate the enthalpy, sample mass was chosen according to the characteristics of each group; summation of mass of PEG and water was used for the calculation of $T_{c1}$ group, mass of water for $T_{c2}$ groups and mass of PEG for $T_{c2}$ group. The reason why the above method was chosen will be described in the latter section of this paper.

The same samples as shown in Fig. 1 were heated at 10 K min$^{-1}$ in a temperature range from 150 to 350 K. Representative heating curves of PEG–water systems are shown in Fig. 4. DSC heating curves vary in a complex manner are com-

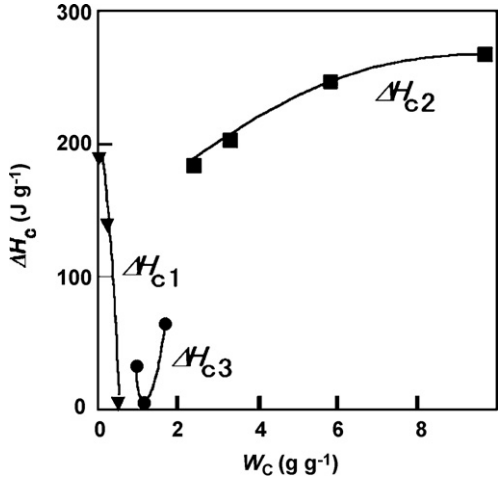


Fig. 3. Relationships between crystallization enthalpies and water content. (●) Crystallization categorized into group 1; (■) group 2; (▼) group 3.

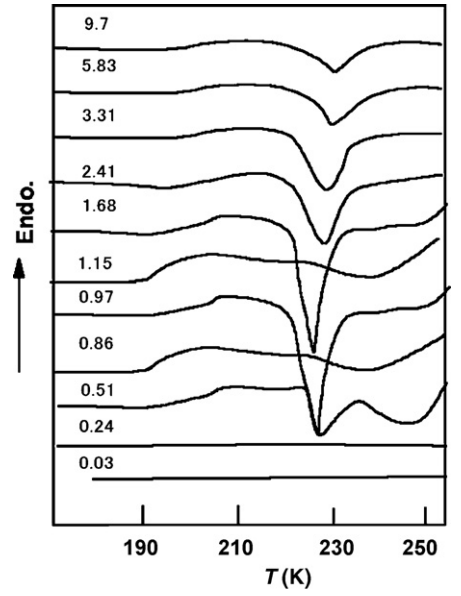


Fig. 5. Magnified DSC curves in a temperature from 170 to 250 K. Numerals in the figure show water content ($W_c$) in g g$^{-1}$.

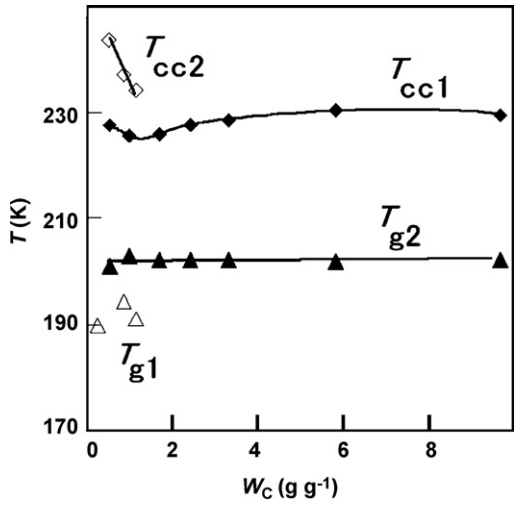


Fig. 6. Relationships between glass transition temperature ($T_g$), cold crystallization temperature ($T_{cc}$) and water content ($W_c$). (♦) Cold crystallization categorized into group 1; (◊) cold crystallization categorized into group 2; (△) glass transition temperature categorized into group 1; (▲) glass transition temperature categorized into group 2.

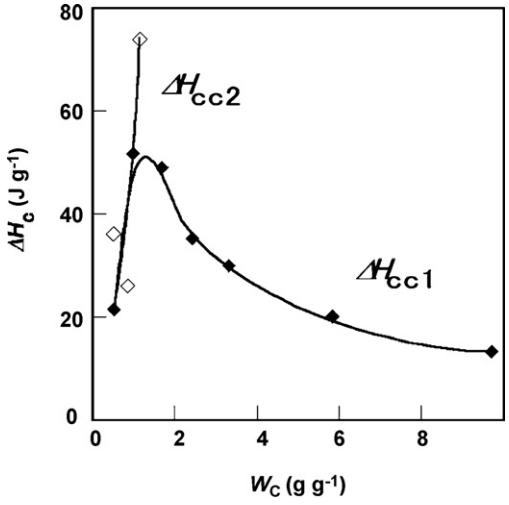


Fig. 8. Relationship between enthalpy of cold crystallization ($\Delta H_{cc}$) and water content. (♦) $\Delta H_{cc}$ of group 1; (◊) $\Delta H_{cc}$ of group 2.

pared with the cooling curves. From the low- to high-temperature side, glass transition, cold crystallization and three kinds of melting are observed. In order to analyze data more precisely, DSC curves from 170 to 250 K are magnified as shown in Fig. 5. In DSC heating curves of the sample having a water content from 0.51 to 1.15 g g$^{-1}$, two kinds of cold crystallization are observed in irregular order, i.e. broad exothermic peak from 230 to 240 K, and sharp exothermic peak at around 230 K. When broad cold crystallization peak is observed, $T_g$ is observed at around 290 K and sharp crystallization peak is observed at around 200 K.

When $T_g$ and $T_{cc}$ are plotted against $W_c$, it is clearly recognized that both $T_g$ and $T_{cc}$ can be categorized in two groups as shown in Fig. 6. One group of $T_g$ and $T_{cc}$ can be found in a water content from 0.5 to 1.2 g g$^{-1}$ where $T_g$ maintains an almost constant value at around 193 K and $T_{cc}$ decrease with increasing $W_c$.

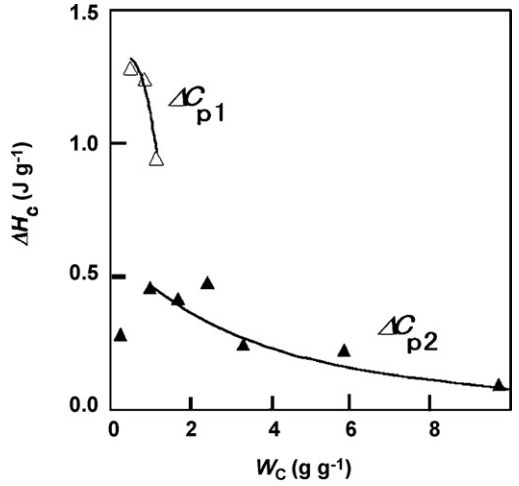


Fig. 7. Relationship between heat capacity difference at $T_g(\Delta C_p)$ and water content. (△) $\Delta C_p$ categorized into group 1; (▲) $\Delta C_p$ categorized into group 2.

The second group, both $T_g$ and $T_{cc}$ maintain at almost the same temperature in a $W_c$ from 1.0 to 10 g g$^{-1}$.

Fig. 7 shows the heat capacity difference at $T_g(\Delta C_p)$. $\Delta C_p$ values can also be categorized into two groups in the same manner as $T_g$ values shown in Fig. 6. As shown in Fig. 7, $\Delta C_p$ values of the group 1 ($\Delta C_{p1}$) are large; in contrast, those of the second group ($\Delta C_{p2}$) are small. Enthalpy values of cold crystallization are shown in Fig. 8. $\Delta H_{cc}$ corresponds to the variation of $T_c$. The maximum value is observed for the second group at around $W_c$ = 1.5 g g$^{-1}$. Results shown in Figs. 7 and 8 strongly suggest that molecular motion of the amorphous part of the system is categorized into two groups.

Fig. 9 shows the magnified DSC heating curves of PEG–water systems in a temperature range from 240 to 330 K. Three kinds of

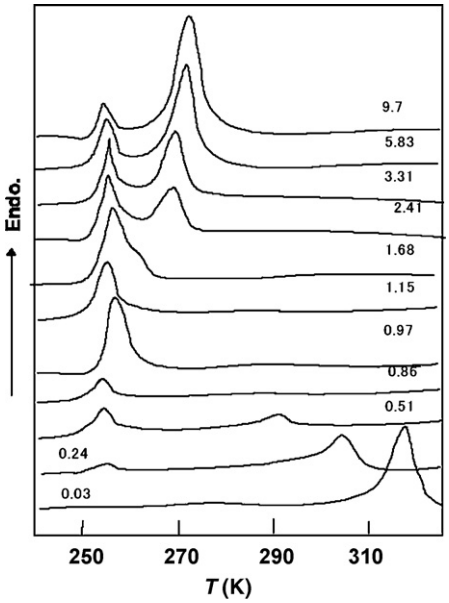


Fig. 9. Magnified DSC heating curves from 240 to 330 K. Numerals in the figure show water content ($W_c$) in g g$^{-1}$.

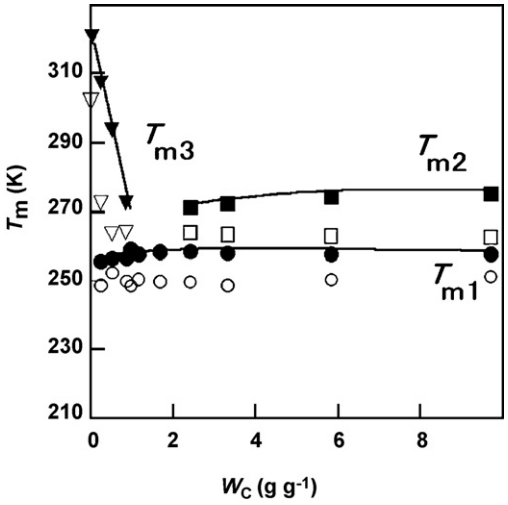


Fig. 10. Relationships between melting temperatures and water content. (●) Melting peak temperature of group 1; (◯) starting temperature of melting; (■) melting peak temperature of group 2; (□) starting temperature of melting; (▼) melting peak temperature of group 3; (▽) starting temperature of melting.

melting can clearly be seen. A large difference is found between crystallization curves shown in Fig. 1 and heating curves in Fig. 9, i.e. the crystallization peak categorized into group 1 can be observed in a narrow $W_c$ range in Fig. 2, in contrast, melting peak of group 1 can be found in a wide $W_c$ range from 0.24 to 9.7 g g$^{-1}$.

Fig. 10 shows the melting temperatures ($T_m$) and starting temperatures of melting ($T_{mi}$) as a function of water content ($W_c$). Melting temperatures of groups 1 and 2 maintain constant values against $W_c$, in contrast, melting temperatures categorized into group 3 decrease linearly. Enthalpies of melting vary in a characteristic manner for each group as shown in Fig. 11. Values of $\Delta H_m$ of group 1 show the maximum value at around 1.5–2.0 g g$^{-1}$. It is noted that variation of $\Delta H_m$ of group 1 is similar to that of $\Delta H_{cc}$, although absolute values of $\Delta H_m$ are larger than those of $\Delta H_{cc}$. Values of $\Delta H_m$ of group 3 decrease linearly and those of group 2 increase with increasing $W_c$.

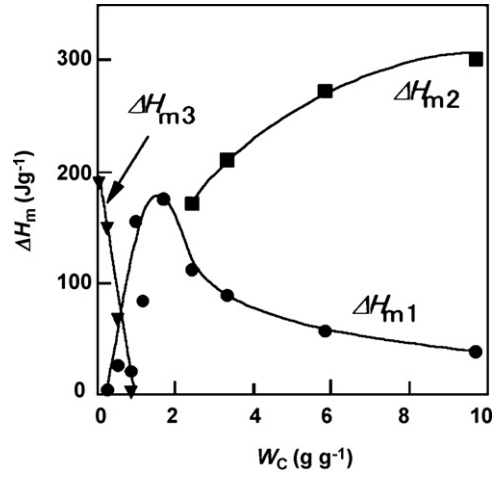


Fig. 11. Relationships between melting enthalpies and water content. (●) Melting enthalpy of group 1; (■) melting enthalpy of group 2; (▼) melting enthalpy of group 3.

## 4. Discussion

### 4.1. Melting and crystallization of PEG crystal

The X-ray analysis showed that the conformation of poly(ethylene oxide) (PEO) is the (7/2) helix consisting of TTG sequences arranging in the planer zigzag form [40]. It is considered that the flexibility of PEO molecular chains is attributable to the considerable distortion from the helical symmetry. Accordingly, PEO is capable to form various crystalline complexes with small molecules [40]. The molecular mass of PEG used in this study is far smaller than that of reported PEO [41,42]. However, if it is assumed that the molecular conformation of PEG is the same as reported one [40] and takes an extended chain crystalline form, the length of each molecular chain of the PEG sample is ca. 9.7 nm. This indicates that spherulite is difficult to be formed when the molecular mobility of the end groups is taken into consideration. At the same time, it is considered that the molecular chains are difficult to take enthangled structure in a similar manner as amorphous polymers having large molecular mass at a temperature higher than glass transition temperature, since characteristic feature of oligomers is found in this mass range [43].

Several researchers have reported the melting behaviour of PEG–water systems. They established phase diagram of PEG–water systems in a water content ranged from 0 to 20 g g$^{-1}$, although the definition of water content is different [30,31]. When previously reported data on melting temperatures were plotted together with our present data shown in Fig. 10, no large difference was observed among melting temperatures. On this account, in this study, we focus on glass transition, cold crystallization and the balance of enthalpy of PEG–water systems.

When a small amount of water is added to PEG, the crystalline region decreases. It is noted that both $\Delta H_{c3}$ and $\Delta H_{m3}$ decrease with increasing water content and also that the values of $\Delta H_{c3}$ and $\Delta H_{m3}$ were identical. Although crystallization temperatures are 10 K lower than melting peak temperatures due to super cooling, both $T_{c3}$ and $T_{m3}$ depend on $W_c$ in a similar manner. Kitano investigated time evolution of FTIR of water sorbed on PEG and reported that bridging water molecules firstly equilibrated in matrix [37]. It is quite reasonable to accept that water molecules diffuse into the crystalline region of PEG and that the crystallinity decreases with increasing water content. On this account, it is appropriate to consider that the crystallization and melting peaks observed at the high-temperature side (group 3) are attributable to phase transition of PEG crystal. The decrease of $\Delta H_{c3}$ and $\Delta H_{m3}$ is considered to be attributed to the fact that the crystalline region decreases with increasing water molecules which are restrained around oxygen via hydrogen bonding [37]. Effect of molecular mass on melting temperature and enthalpy is also noteworthy, especially the molecular mass of PEG used in this study is in an oligomeric region [34,42].

### 4.2. Glass transition of amorphous region of PEG in the presence of water

A part of PEG solved in water in the above systems forms an amorphous region and freezes in the glassy state at a temperature lower than $T_g$. Glass transition is observed in both cooling and heating curves at around 193 K in a $W_c$ range from 0.24 to 1.25 g g$^{-1}$. As shown in Figs. 5 and 6, the systems showing the low-temperature $T_g$ crystallize at the high-temperature $T_{cc}$. The high-temperature $T_{cc}$ suggests that remained crystallites restrict the free molecular motion of amorphous PEG molecules associating with water molecules. As shown in Fig. 3, $T_{c3}$ is clearly detected in DSC heating curves for the samples with $W_c$ 0.24 and 0.51 g g$^{-1}$. This suggests that the crystalline region of PEG remains in the samples. When $W_c$ increased, PEG crystals disappear and ice is gradually formed in the system.

The fact that glass transition is significantly observed in the cooling process suggests that the glassy state is readily formed in the PEG–water system even if cooling rate is not high. Heat capacity difference at $T_g$($\Delta C_p$) calculated from both heating and cooling curves is large compared with those of ordinary amorphous polymers [44]. In our previous reports [39], we calculated $\Delta C_p$ values of water–polysaccharide systems assuming that the restrained water homogeneously mixed with saccharide and the mixture forms amorphous ice at a temperature lower than $T_g$. Heat capacity difference at $T_g$ of amorphous ice is reported to be 4 J g$^{-1}$ K$^{-1}$ [39] which contributes to large $\Delta C_p$ values. Large values of PEG–water systems are also explained by the above mechanism.

It is well established that glass transition is a relaxation phenomenon having a certain distribution of relaxation time. The fact that the baseline at around glass transition gradually changes suggests that amorphous structure of PEG–water systems inherits a certain distribution of relaxation time (Fig. 5). It is thought that $T_{g2}$ of PEG–water systems is reasonable to be defined by the procedure described in the experimental section. The fact that the $T_{g2}$ value maintained at round 200 K regardless of $W_c$ (Fig. 6) may come from the molecular conformation of PEG pentamer. Furthermore, the fact that $T_g$ is detected in the presence of a large amount of ice in the system suggests that free molecular motion of oligomeric PEG restrained with water molecules via hydrogen bonding readily enhance molecular rearrangement which is observed as cold crystallization.

### 4.3. Cold crystallization

Cold crystallization is observed for PEG–water systems in a wide range of water contents. With increasing $W_c$, PEG molecules associating with amorphous ice rearrange more freely and $T_{cc}$ shifts to the low-temperature side. It is noteworthy that the high-temperature side $T_g$($T_{g2}$) can be detected in a wide $W_c$ range of PEG–water systems, even though $\Delta C_p$ values decreases with increasing $W_c$ as shown in Fig. 7 are small. In other polysaccharide–water systems, $T_g$ can hardly be detected when water content exceeds 3.0 g g$^{-1}$ [22] due to the fact that the free molecular motion of amorphous chains is restricted by hexagonal ice formed in the system. In the cooling curves of PEG–water systems, crystallization of ice ($T_{c2}$) is observed from the $W_c$ at around 2.0 g g$^{-1}$ as shown in Fig. 2. It is remarkable that glass transition is observed in the presence of a large amount of ice in this system.

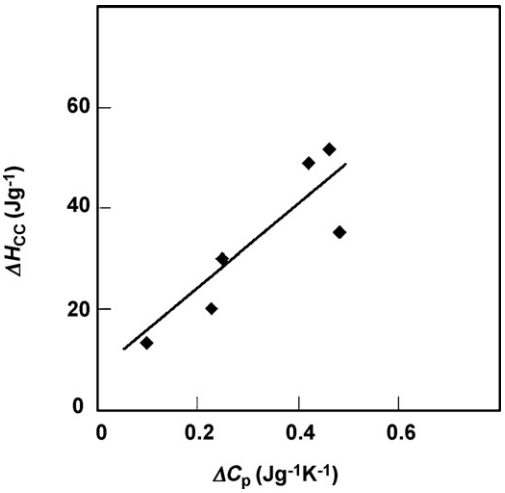


Fig. 12. Relationship between $\Delta C_p$ at high-temperature side $T_g$ and $\Delta H_{cc}$.

Fig. 12 shows the relationship between $\Delta C_p$ at high-temperature side $T_{g2}$ and $\Delta H_{cc}$. The linear relationship indicates that the amorphous chain rearranges and forms eutectic crystals at $T_{cc}$. It is clear that the amount of glassy PEG–water systems increases, $\Delta H_{m1}$ increases (Fig. 11). This relationship indicates that the high-temperature side $T_g$ and $T_{cc}$, as shown in Fig. 5, strongly correlate with crystallization of PEG–water eutectic crystal.

Enthalpy of melting of eutectic crystals ($\Delta H_{m1}$) shows the maximum value at around 1.8 g g$^{-1}$ as shown in Fig. 11. When molecular mass of repeating unit of PEG and the water content showing the maximum are taken in consideration, glassy PEG molecules associating with 4 mol of water per repeating unit bring about the largest amount of eutectic crystal. With increasing $W_c$, hexagonal ice is grown and the amount of eutectic crystals decreases. When $\Delta H_{cc}$ curves (Fig. 8) are compared with those of $\Delta H_{m1}$ (Fig. 11), the maximum point of both curves is found at the same $W_c$. Curves of $\Delta H_{cc}$ and $\Delta H_{m1}$ vary in a

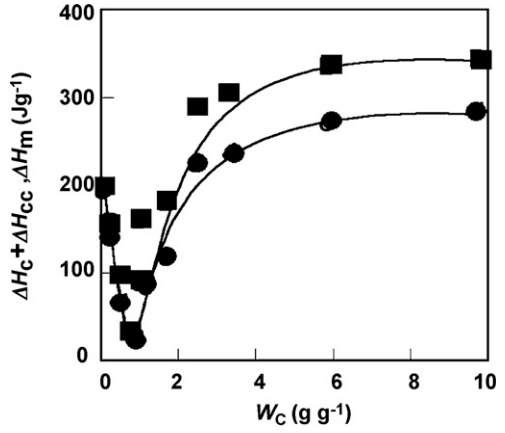


Fig. 13. Relationship between $\Delta H_m$, $\Delta H_{cc} + \Delta H_c$ and $W_c$. (■) $\Delta H_m$; (●) $\Delta H_{cc} + \Delta H_c$.

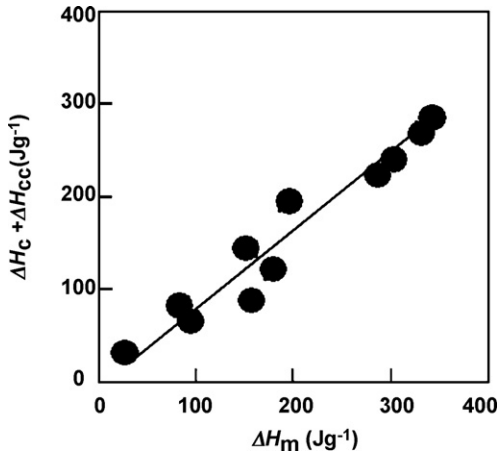


Fig. 14. Relationship between $\Delta H_m$ and $\Delta H_{cc} + \Delta H_c$.

similar manner as a function of $W_c$, although absolute enthalpy values of $\Delta H_{cc}$ are smaller than those of $\Delta H_m$. This similarity suggests that $T_{m1}$ is the melting temperature of crystals formed at the cold crystallization. It is considered that the enthalpy difference is the result of several factors: one is that mass value used for enthalpy calculation of cold crystallization is large since calculation was carried out assuming all PEG and water concern the above event, and the other is that molecular ordering proceeds during heating in a temperature from $T_{cc}$ to $T_{m1}$.

### 4.4. Enthalpy balance

Fig. 13 shows the relationships between $\Delta H_m$ ($=\Delta H_{m1} + \Delta H_{m2} + \Delta H_{m3}$), $(\Delta H_c + \Delta H_{cc})$ and $W_c$. It is clearly seen that both curves vary in a similar manner, although $\Delta H_m$ is always larger than those of $(\Delta H_c + \Delta H_{cc})$ due to the reasons described above. When $\Delta H_m$ is related with $(\Delta H_c + \Delta H_{cc})$, linear relationship is established as shown in Fig. 14. The results of Figs. 10 and 11 indicate that enthalpies of melting and crystallization are well balanced, if we accept that amorphous ice associated with PEG molecules crystallizes at $T_{cc}$.

## 5. Conclusion

From the above facts, it is concluded that cold crystallization is attributable to the molecular rearrangement of PEG molecules associated with amorphous ice. When the four water molecules are attached to one repeating unit of PEG, the heat capacity difference at glass transition temperature becomes the largest and the enthalpy of cold crystallization shows the maximum value. As described in the introductory section, PMEA is also known to show stable cold crystallization in DSC heating curves. Although PMEA is a water insoluble amorphous polymer, a major part of bound water freezes as amorphous ice similar to the PEG–water system [9,12,13]. Biocompatible characteristics observed in both PMEA and PEG is closely related with the existence of a large amount of amorphous ice in the systems [13]. Cold crystallization can be observed for the systems, in which a portion of water molecules is dominantly restrained as non-freezing water and the major portion of bound water freezes in glassy state homogeneously associated with amorphous PEG molecules. In order to design polymers having good biocompatibility, stable cold crystallization that appeared in the DSC curves is thought to be an index for screening.

## References

[1] Y. Iwasaki, Y. Aiba, N. Morimoto, Y. Nakabayashi, K. Ishihara, Semi-interpenetrating polymer networks composed of biocompatible phospholipids polymer and segmented polyurethane, J. Biomed. Mater. Res. 52 (2000) 701–708.
[2] Y. Mori, S. Nagaoka, T. Takiguchi, T. Kikuchi, N. Noguchi, H.Y. Tanzawa, A. Noishik, New antithrombogenic material with long polyethylene oxide chain, Trans. Am. Soc. Artif. Intern. Organs 28 (1982) 459–463.
[3] N.A. Peppas (Ed.), Hydrogel in Medicine and Pharmacy, vol. 2, CRC Press, Boca Raton, FL, 1987.
[4] T. Okano, S. Nishiyama, I. Shinohara, T. Akaike, Y. Sakurai, K. Kataoka, T. Tsuruta, Effect of hydrophilic and hydrophobic micro-domains on mode of interaction between block copolymer and blob platelets, J. Biomed. Mater. Res. 15 (1981) 393–403.
[5] D. Severian (Ed.), Polymeric Biomaterials, Mercel Dekker Inc., New York, 2002.
[6] T. Tsuruta, Contemporary topics in polymeric materials for biomedical applications, Adv. Polym. Sci. 126 (1996) 1–51.
[7] M. Tanaka, T. Motomura, M. Kawada, T. Anzai, Y. Kasori, T. Shiroya, K. Shimura, M. Onishi, A. Mochizuki, Blood compatible aspects of poly(2-methoxyethylacrylate) (PMEA). Relationship between protein adsorption and platelet adhesion on PMEA surface, Biomaterials 21 (2000) 1471–1481.
[8] M. Tanaka, T. Motomura, M. Kawada, T. Anzai, Y. Kasori, K. Shimura, M. Onishi, A. Mochizuki, Y. Okahata, A new blood compatible surface prepared by poly(2-methoxyethylacrylate) (PMEA) coating protein adsorption on PMEA surface, Jpn. J. Artif. Organs 29 (2000) 209–216.
[9] M. Tanaka, T. Motomura, N. Ishii, K. Shimura, M. Onishi, A. Mochizuki, T. Hatakeyama, Cold crystallization of water inhydrated poly(2-methoxyethyl acrylate), Polym. Int. 49 (2000) 1709–1713.
[10] M. Tanaka, A. Mochizuki, T. Motomura, K. Shimura, A. Onishi, Y. Okahata, In situ studies on protein adsorption onto a poly(2-methoxyethyl acrylate) surface by a quartz crystal microbalance, Colloids Surf. A 193 (2001) 145–152.
[11] M. Tanaka, A. Mochizuki, T. Shiroya, T. Motomura, K. Shimura, A. Onishi, Y. Okahata, Study on kinetics of protein adsorption and desorption on poly(2-methoxyethyl acrylate) (PMEA) surface, Colloids Surf. A 203 (2002) 195–204.
[12] M. Tanaka, A. Mochizuki, N. Ishii, T. Motomura, T. Hatakeyama, Study on blood compatibility of poly(2-methoxyethyl acrylate). Relationship between water structure and platelet compatibility in poly(2-methoxyethyl acrylate-co-2-hydroxyethylmethacrylate), Biomacromolecules 3 (2002) 36–41.
[13] M. Tanaka, A. Mochizuki, Effect of water structure on blood compatibility—thermal analysis of water in poly(meth)acrylate, J. Biomed. Mater. Res. A 68 (4) (2004) 684–695.
[14] T. Anzai, A. Okumura, M. Kawaura, K. Yokoyma, H. Oshiyama, T. Kido, C. Nojiri, Evaluation of the biocompatibility of an in vitro test using a poly(2-methoxyathy acrylate) coated oxygenators, Jpn. J. Artif. Organs 9 (2000) 73–77.
[15] D. Baykut, F. Bernet, J. Wehrle, K. Weichelt, P. Schwartz, H.R. Zerkowski, New surface biopolymers for oxygenators: anin vitro hemocompatibility test of poly(2-methoxyethylacrylate), Eur. J. Med. Res. 30 (2001) 297–305.
[16] X.M. Mueller, D. Jegger, M. Augstburger, J. Horisberger, L.K. von Segesser, Poly2-methoxyethyl acrylate (PMEA) coated oxygenator: an ex vivo study, Int. J. Artif. Organs 25 (2002) 223–229.
[17] N. Saito, S. Motoyam, J. Sawamoto, Effects of new polymer coated extracorporeal circuits on biocompatibility during cardiopulmonary bypass, Artif. Organs 24 (2000) 547–554.

[18] H. Suhara, Y. Sawa, M. Nishimura, H. Oshiyama, K. Yokoyama, N. Saito, H. Matsuda, Efficacy of a new coating material, PMEA, for cardiopulmonary bypass circuits in a porcine model, Ann. Thorac. Surg. 71 (2001) 1603–1608.
[19] B.L. Greenfeld, K.R. Brinkman, K.L. Koziol, M.W. McCann, MerriganKA, L.P. Steffen, K.A. Woods, A.H. Stammers, L.M. Hock, The effect of surface modification and aprotinin on cellular injury during simulated cardiopulmonary bypass, J. Extra Corpor. Technol. 34 (2002) 267– 270.
[20] C.F. Hazlewood, B.L. Nichols, N.F. Chamberlain, Evidence for the existence of a minimum of two phases of ordered water in skeletal muscle, Nature 222 (1969) 747–750.
[21] J. Israelachivili, H. Wennerstrom, Role of hydration and water structure in biological and colloidal interactions, Nature 379 (1996) 219–225.
[22] H. Uedaira, Water in biological systems, in: B. Pullman, K. Yagi (Eds.), Water and Metal Cations in Biological Systems, Japan Scientific Societies Press, Tokyo, 1980, pp. 47–56.
[23] T. Hatakeyama, H. Hatakeyama, Interaction between water and hydrophilic polymers, Thermochim. Acta 308 (1998) 3–22.
[24] T. Hatakeyama, Y. Ikeda, H. Hatakeyama, Effect of bound water on structural change of regenerated cellulose, Makromol. Chem. 188 (1987) 1875–1884.
[25] T. Hatakeyama, H. Hatakeyama, Thermal Properties of Green Polymers and Biocomposites, Kluwer Academic Publishers, Dordrecht,2004.
[26] T. Hatakeyama, S. Naoi, H. Hatakeyama, Phase transition of locust bean gum–, tara gum– and guar gum–water systems, J. Therm. Anal. Calorim. 70 (2002) 841–852.
[27] H. Yoshida, T. Hatakeyama, H. Hatakeyama, Phase transitions of the water–xanthan system, Polymers 31 (1990) 693–698.
[28] T. Hatakeyama, H. Yoshida, H. Hatakeyama, A differential scanning calorimetry study of the phase transition of the water–sodium cellulose sulfate system, Polymers 28 (1987) 1282–1286.
[29] T. Hatakeyama, H. Hatakeyama, Molecular relaxation of cellulosic polyelectrolytes with water. Viscoelasticity of biomaterials, in: W.G. Glasser, H. Hatakeyama (Eds.), ACS Symposium Series 489, ACS, Washington DC, 1992, pp. 329–340.
[30] N.B. Graham, M. Zulfigar, N.E. Nwachuku, A. Rashid, Interaction of poly(ethylene oxide) with solvents. 2. Interaction of water with poly(ethylene glycol), Polymers 30 (1989) 528–533.
[31] L. Huang, K. Nishinari, Interaction between poly(ethylene glycol) and water as studied by differential scanning calorimetry, J. Appl. Polym. Sci. B 39 (2001) 496–506.
[32] J.M. Harris (Ed.), Poly(ethylene glycol) chemistry, biotechnical and biomedical applications, Plenum Press, New York, 1992.
[33] M.M. Feldstein, G.A. Shandryuk, S.A. Kuprsov, N. APlaté, Coherence of thermal transitions in poly(*N*-vinyl pyrrolidone)–(poly(ethylene glycol) compatible blends. I. Interrelations among the temperatures of melting, maximum cold crystallization rate and glass transition, Polymers 41 (2000) 5327–5338.
[34] M.M. Feldstein, S.A. Kuprsov, G.A. Shandryuk, Coherence of thermal transitions in poly(*N*-vinyl pyrrolidone)–(poly(ethylene glycol) compatible blends. II. The temperatures of maximum cold crystallization rate versus glass transition, Polymers 41 (2000) 5339–5348.
[35] W.Y. Huang, S. Matsuoka, T.K. Kwei, Y. Okamaoto, X. Hu, M.H. Rafailovich, J. Sokolov, Organization and orientation of a triblock copolymer poly(ethylene glycol)–*b*-poly(*p*-phenylene ethynylene)–*b*-poly(ethylene glycol) and its blends in thin films, Macromolecules 34 (2001) 7809–7816.
[36] K.B. Keys, F.M. Andreopoulos, N.A. Peppas, Poly(ethylene glycol) star polymer hydrogels, Macromolecules 31 (1998) 8149–8156.
[37] H. Kitano, K. Ichikawa, M. Ide, M. Fukuda, W. Mizuno, Fourier transform infrared study on the state of water sorbed on poly(ethylene glycol) films, Langmuir 17 (2001) 1889–1895.
[38] T. Hatakeyama, F.X. Quinn, Thermal Analysis, Fundamentals and Applications to Polymer Science, 2nd ed., John Wiley, UK, 1999.
[39] H. Yoshida, T. Hatakeyama, H. Hatakeyama, Effect of water on the main chain motion of polysaccharide hydrogels. Viscoelasticity of biomaterials, in: W.G. Glasser, H. Hatakeyama (Eds.), ACS Symposium Series 489, ACS, Washington, 1992, pp. 218–230.
[40] Y. Takahashi, H. Tadokoro, Structural studies of polyethers, $(–(CH_2)m–O)_n$. X. Crystal structure of poly(ethylene oxide), Macromolecules 6 (1973) 672–675.
[41] S.Z.D. Cheng, J.B. Barley, P.A. Giusti, Spherulite formation in poly(ethylene oxide) mixtures, Polymers 31 (1990) 845–849.
[42] K. Pielichowski, K. Flejtuch, J. Pielichowski, Step-scan alternation DSC study of melting and crystallization in poly(ethylene oxide), Polymers 45 (1994) 1235–1242.
[43] T. Hatakeyama, M. Serizawa, Glass transition of oligostyrene with different end groups, Polym. J. 14 (1982) 51–57.
[44] T. Hatakeyama, H. Hatakeyama, Effect of chemical structure of amorphous polymers on heat capacity difference at glass transition temperature, Thermochim. Acta 267 (1995) 249–257.